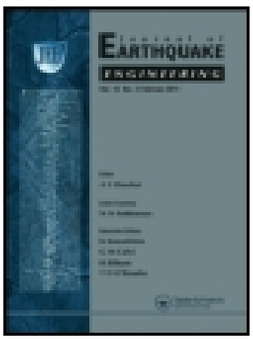

Journal of Earthquake Engineering

ISSN: 1363-2469 (Print) 1559-808X (Online) Journal homepage: https://www.tandfonline.com/loi/ueqe20

Implementation of Bond-Slip Performance Models in the Analyses of Non-Ductile Reinforced Concrete Frames Under Dynamic Loads

Jiuk Shin, Lauren K. Stewart, Chuang-Sheng Yang & David W. Scott

To cite this article: Jiuk Shin, Lauren K. Stewart, Chuang-Sheng Yang & David W. Scott (2017): Implementation of Bond-Slip Performance Models in the Analyses of Non-Ductile Reinforced Concrete Frames Under Dynamic Loads, Journal of Earthquake Engineering, DOI: 10.1080/13632469.2017.1401565

To link to this article: https://doi.org/10.1080/13632469.2017.1401565

Published online: 27 Dec 2017.

Submit your article to this journal

Article views: 131

View Crossmark data

Full Terms & Conditions of access and use can be found at
https://www.tandfonline.com/action/journalInformation?journalCode=ueqe20

JOURNAL OF EARTHQUAKE ENGINEERING
https://doi.org/10.1080/13632469.2017.1401565

Taylor & Francis
Taylor & Francis Group

Check for updates

Implementation of Bond-Slip Performance Models in the Analyses of Non-Ductile Reinforced Concrete Frames Under Dynamic Loads

Jiuk Shin, Lauren K. Stewart, Chuang-Sheng Yang, and David W. Scott

School of Civil and Environmental Engineering, Georgia Institute of Technology, Atlanta, GA USA

ABSTRACT

Non-ductile reinforced concrete frames have seismic vulnerabilities due to inadequate reinforcing details. Adequately characterizing the performance of these details is critical to the development of analytical models. This study presents a methodology to simulate the response of such frames with and without fiber-reinforced polymer column jackets. The bond-slip effects between reinforcing bars and surrounding concrete, observed in column lap-splice and beam–column joints, are modeled with one-dimensional slide line models in LS-DYNA. The model is defined from failure modes and bonding conditions observed in full-scale dynamic tests and can predict story displacements, inter-story drifts, and damage mechanisms.

ARTICLE HISTORY
Received 24 November 2016
Revised 22 August 2017
Accepted 2 November 2017

KEYWORDS
Non-Ductile Reinforced Concrete Frame; Fiber-Reinforced Polymer Column Jacket; Finite Element; Bond-Slip Effect; Full-Scale Dynamic Test

1. Introduction

Reinforced concrete (RC) building structures constructed before the 1970s were typically designed only for gravity loads. This design practice led to seismically deficient detailing in columns and beam–column joints, such as small-diameter and largely spaced transverse reinforcement in columns, insufficient length of column lap-splice bars, and inadequate detailing of beam–column joints (e.g. no transverse reinforcing bars in panel zones, straight anchorage of positive beam reinforcing bars, and discontinuous positive beam reinforcing bars) [Bracci *et al.*, 1995; El-Attar *et al.*, 1997; Priestley, 1997; Wright, 2015]. Such inadequate reinforcement details can result in a poor bond-slip condition between the reinforcing bars and the surrounding concrete observed in both column lap-slices and beam–column joints. Post-earthquake reconnaissance reports [Aschheim *et al.*, 2000; Sezen *et al.*, 2000] have demonstrated that inadequate reinforcement details in columns and beam–column joints can lead to premature collapse of the structure. For example, the 1999 Kocaeli earthquake in Turkey led to the collapse of multiple RC building structures designed without appropriate seismic detailing of reinforcement. Many of these collapses were attributed to shear and/or lap-splice failures in columns, in addition to the development of significant damage in beam–column joints.

To prevent the premature failure of non-ductile RC frame structures, seismic retrofit techniques for RC columns using fiber-reinforced polymer (FRP) composites have been widely used [Seible *et al.*, 1997; Xiao *et al.*, 1999; Haroun *et al.*, 2003; Sause *et al.*, 2004;

CONTACT Lauren K. Stewart lauren.stewart@ce.gatech.edu School of Civil and Environmental Engineering, Georgia Institute of Technology, Atlanta, GA 30332, USA.

Color versions of one or more of the figures in the article can be found online at www.tandfonline.com/ueqe.

© 2017 Taylor & Francis Group, LLC

ElGawady *et al.*, 2010; Yan and Pantelides, 2011; Shin *et al.*, 2016]. These previous experimental studies have demonstrated that FRP column jackets can enhance the flexural, shear, and lap-splice capacities of non-ductile RC columns as well as increase the buckling resistance of reinforcing bars by providing additional confining pressure. A recent study [Shin *et al.*, 2016] performed a series of seismic dynamic tests for a full-scale, two-story non-ductile RC test frame, designed for only gravity loads, in non-retrofitted (referred to as "as-built test frame") and retrofitted (referred to as "retrofitted test frame") configurations, to investigate the dynamic responses under seismic loading. For the retrofitted test frame, prefabricated FRP column jackets were installed on the first-story columns in the full-scale test frame as a retrofit system. By comparing the dynamic responses between the as-built and retrofitted test frames, the effectiveness of the retrofit system was demonstrated in terms of inter-story drifts, column rotations, and drift concentration factors (DCFs).

This paper aims to validate the dynamic responses of full-scale, non-ductile, and retrofitted test frames in terms of damage, story displacements, and inter-story drifts using finite element (FE) frame models. The FE frame models are developed with the nonlinear explicit analysis program, LS-DYNA [2013]. The numerical models are verified with the measured responses from a series of full-scale dynamic tests [Wright, 2015; Shin *et al.*, 2016]. Based on the dynamic responses measured from the full-scale tests, this study identifies true bond-slip behavior in individual column lap-splice and panel zones for both the as-built and retrofitted test frames. To represent the bond-slip behavior observed in the full-scale dynamic testing, a modeling methodology that characterizes bond-slip performance using LS-DYNA is proposed and incorporated into the FE frame models. This empirical bond-slip performance behavior is simulated with a one-dimensional slide line model. The modeling methodology for representing the bond-slip performance is applicable for implementation in analyses of other structures with similar, seismically deficient detailing. Additionally, the effect of changing parameters on the bond-slip performance of the FE frame models is investigated. Previous works involving FE analysis on RC frames usually focused on the validation of experimental responses under a quasi-static monotonic or cyclic load at the element or basic system level, such as non-ductile and FRP-confined RC columns [Kwon and Spacone, 2002; Hu *et al.*, 2003], and RC beam–column joints [Deaton, 2013]. This study verifies the proposed modeling methodology at the frame level with the full-scale dynamic experimental results.

2. Full-Scale Dynamic Testing of As-Built and Retrofitted RC Test Frames

2.1. *Description of Full-Scale Test Frames and Test Setup*

A series of full-scale dynamic tests were performed on four identical two-story, two-bay, non-ductile RC test frames constructed at the Georgia Institute of Technology (see Figure 1a). One test frame was constructed and tested in an as-built configuration, and one test frame was retrofitted with prefabricated FRP column jackets on the first-story columns (see Figure 1b). The identical RC test frames were designed in accordance with ACI 318-63 [1963]. Since this building code has no seismic requirements, the test frames were composed of inadequate reinforcement details in columns and beam–column joints. The design included short column lap-splice lengths, poor confinement, and weak column strong beam (WCSB) systems. The seismically deficient reinforcement details of the RC test frames are summarized in Figure 2.

Figure 1. Full-scale, two-story two-bay non-ductile RC test frames: (a) four identical full-scale test frames; (b) FRP jacketed column in the retrofitted test frame; (c) hydraulic linear shaker on the roof of the RC test frames [Shin *et al.*, 2016].

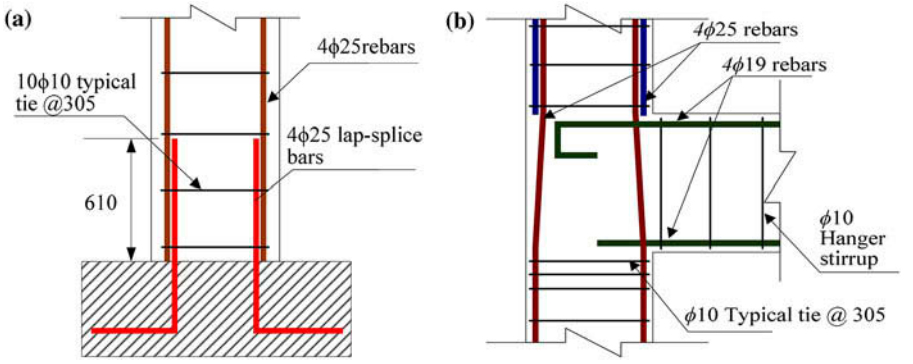

Figure 2. Reinforcement details of the full-scale, as-built test frame: (a) first-story column; and (b) first-story exterior beam–column joint [Wright, 2015].

To enhance the ductility, shear, and lap-splice capacities of the as-built test frame, an FRP jacket system was designed using the retrofit design process proposed by Seible *et al.* [1997]. Additionally, as specified in Federal Emergency Management Agency (FEMA) 547 [2006], gaps of approximately 13 mm were left at the top and bottom of the column to prevent the interaction between the FRP jacket and the adjacent elements (e.g. slab, beam, and foundation). The test frames were excited beyond their linear elastic limit using a mobile shaker

system [NEES@UCLA, 2015] installed on the roof of the test frames as shown in Figure 1c. The mobile shaker sequentially applied seismic (1940 El Centro earthquake) and sine motions to the test frames. Story displacements, hinge rotations, accelerations, and bar strains induced by the top excitation were measured. Additional information related to the experimental setup of the as-built and retrofitted test frames can be found in Wright [2015] and Shin *et al.* [2016], respectively.

2.2. *Experimental Results*

At the completion of the dynamic loading sequences, the as-built test frame was severely damaged in the first-story columns and exhibited mechanisms such as vertical splitting cracks along the column lap-splice bars and shear cracks within the column lap-splice regions. No damage was detected in the second story. The lap-splice failure in the first-story column bases and the pullout failure in the first-story exterior beam–column joints were demonstrated by the measured relation between the hinge rotations and the reinforcing bar strains [Wright, 2015]. Such bond-slip mechanisms significantly contributed to the soft-story behavior of the first story.

3. Methodology for the FE Model

3.1. *Structural Geometry Modeling*

A methodology for modeling the RC frame structure with bond-slip effects was developed and verified with the experimental responses measured by the full-scale dynamic experiments. The test frames were modeled using the nonlinear, explicit FE software LS-DYNA [LSTC, 2013]. Figure 3 shows a three-dimensional view of the as-built and retrofitted FE frame models. As shown in Figure 3a, the FE frame models were developed using a half-symmetry condition, which was used to reduce computational demands. To enforce the condition on the plane of symmetry, the two rotational degrees-of-freedom parallel to the symmetry plane (R_x and R_z in the global coordinate system) and the translational degree-of-freedom perpendicular to the symmetry plane (D_y in the global coordinate system) were restrained. Additionally, the foundation bases were restrained in all translational and rotational directions, which simulated the fixed condition. Live loads in the experiment were simulated by placing steel rails on the second and third floors of the frame. These weights were converted to masses, and then equally distributed as nodal masses on each element of the floor slab using the option Element_Mass in LS-DYNA.

The concrete column and beam models in the longitudinal direction (x-direction) utilized eight-node solid elements with single point integration. All reinforcing bars were modeled using two-node Hughes–Liu beam elements. The longitudinal and transverse reinforcing bars in the column and beam elements were connected to the concrete mesh nodes. The nodes that linked the concrete and reinforcement mesh were shared. These shared nodes were fully bonded; however, to capture bond-slip effects, the lap-splice bars in the columns and straight anchorages in the joint regions have separate nodes from the concrete mesh nodes. These separate nodes were linked with one-dimensional slide lines. Since the foundation, slab, and transverse beam had no significant damage during the dynamic tests, those elements were modeled using shell elements with an elastic material model (MAT001 in LS-DYNA) to develop a more efficient model. The elastic

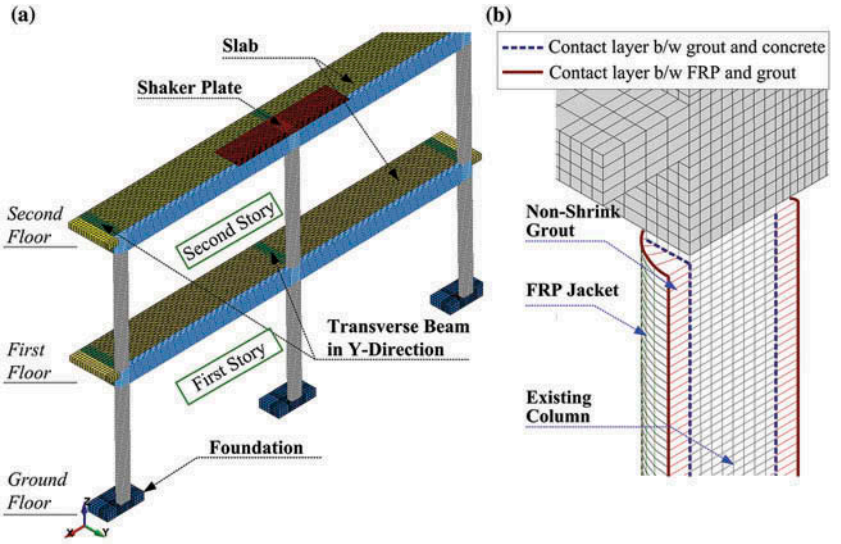

Figure 3. Three-dimensional view of the FE frame models: (a) as-built FE frame model; (b) first-story column of the retrofitted FE frame model.

material model was reduced by stiffness reduction factors specified in ASCE 41-13 [2014]. To impose the shaker forces measured from the full-scale dynamic testing, a shaker plate was placed on the top of the FE frame model. The shaker plate was represented using solid elements with a rigid material (MAT020 in LS-DYNA).

Figure 3b shows the model of the FRP column jacketing system on one of the first-story columns, consisting of non-shrink grout and FRP composite. The non-shrink grout model utilized solid elements to provide additional confining pressures. The FRP jacket model, placed on the surface of the grouting model, was modeled using the shell elements with the corresponding thicknesses to the FRP jackets of the retrofitted test frame: two-layer FRP jacket (1.32 mm in thickness) on the top and bottom of the column, and one-layer FRP jacket (0.66 mm in thickness) in the middle of the column [Shin *et al.*, 2016]. To represent the half-symmetry condition for the retrofitted FE frame model, the FRP jacket and grout elements were restrained in the y-translational direction and the x- and z-rotational directions. Additionally, as illustrated in Figure 3b, the FRP jacket system was assumed to have two different interface layers: a contact layer between the concrete and non-shrink grout models and a contact layer between the non-shrink grout and FRP jacket models. These interface layers were simulated using the LS-DYNA function CONTACT AUTOMATIC SURFACE-TO-SURFACE (referred to as "surface-to-surface contact"), which was developed by Tabiei and Wu [Tabiei and Wu, 2000]. In this contact function, the frictional coefficients of the interface layers were assumed to be 0.8 based on previous works [Moradi, 2007; Davidson, 2008; Lee and Shin, 2016] that recommended the use of coefficient of friction values ranging from 0.6 to 0.9 under dynamic loading. The coefficient of friction value of 0.8 was incorporated into both interface layers between the concrete and non-shrink grout models and between the grout and FRP jacket models.

3.2. Material Models

3.2.1. Concrete Material

To predict the concrete behavior, LS-DYNA provides several material models, such as WINFRITH_CONCRETE (MAT084, often referred to as the "Winfrith model") [Broadhouse, 1986], CSCM (MAT159, referred to as the "CSC model") [Schwer and Murray, 1994], and CONCRETE_DAMAGE_REL3 (MAT072R3) [Malvar *et al.*, 1997; Crawford *et al.*, 2012], which is well known as the Karagozian & Case (K&C) concrete model (referred to as the "KCC model"). These models have a default parameter generation function (e.g. the unconfined compressive strength of the concrete) and capture post-peak strain softening, shear dilation, and confinement effect in concrete behavior. Wu *et al.* [2010] examined the triaxial behavior of a single solid element modeled with three different concrete constitutive models, and compared the simulated results with triaxial compression tests. The numerical study demonstrated that the KCC model can reproduce concrete damage behavior, softening, modulus reduction, shear dilation, and confinement effect under the wide range of confining pressures. Additionally, this KCC model has been extensively verified with the experimental responses obtained from quasi-static, blast, and high-velocity impact loading tests [Wu and Crawford, 2015]. Therefore, this study selected the KCC model to simulate the concrete behavior among the various concrete constitutive models provided in LS-DYNA.

The KCC model is characterized by three independent shear failure surfaces: the maximum surface ($\Delta\sigma_m$), the yield surface ($\Delta\sigma_y$), and the residual surface ($\Delta\sigma_r$). The strain hardening-softening responses in axial stress–strain behavior are established by the combination of three independent shear surfaces and damage function as given in Equations (1) and (2), where σ is axial stress, P is hydrostatic pressure, $\eta(\lambda)$ is damage function, λ is the effective plastic strain, and λ_m is the effective plastic strain corresponding to $\Delta\sigma_m$ [Malvar *et al.*, 1997; Wu and Crawford, 2015].

$$\sigma = \eta(\lambda) \cdot [\Delta\sigma_m(P) - \Delta\sigma_y(P)] + \Delta\sigma_y(P) \; (strain\ hardening)\; \lambda \leq \lambda_m \tag{1}$$

$$\sigma = \eta(\lambda) \cdot [\Delta\sigma_m(P) - \Delta\sigma_r(P)] + \Delta\sigma_r(P) \; (strain\ softening)\; \lambda > \lambda_m \tag{2}$$

The KCC model can simulate a shear dilation using a parameter, ω. This parameter can capture the expansion of concrete as it cracks. If high confinement effects are present in FRP jackets, the ω parameter can contribute to providing a confining pressure, and thus it can increase the strength and ductility [Crawford *et al.*, 2012]. In other words, the ω parameter plays a critical role in simulating reasonable confinement effects. Crawford *et al.* [2013] suggested $\omega = 0.9$ for well-confined concrete components (FRP-jacketed RC column) and $\omega = 0.5$ or 0.75 for poorly confined concrete components (non-ductile RC column). Based on these past studies, this study employed the ω parameter of 0.9 for the retrofitted columns and the ω parameter of 0.5 for the as-built columns. Table 1 shows the main material parameters of the KCC model for the as-built and retrofitted FE frame models. The tensile strength of the concrete materials was computed by the default parameter generation function of the KCC model.

3.2.2. Steel Material

PLASTIC_KINEMATIC (MAT003, referred to as "elasto-plastic material model") has been widely used to simulate steel behavior. The steel stress–strain curve of the elastic-plastic material model represents bilinear behavior with linear isotropic hardening. The

Table 1. Main material parameters of the KCC model.

		As-Built FE frame		Retrofitted FE frame	
Story levels	Element	Concrete strength (MPa)	ω-parameter	Concrete strength (MPa)	ω-parameter
First story	Column	31.5	0.5	32.8	0.9
	Beam	25.0	0.5	26.5	0.5
Second story	Column	28.5	0.5	30.3	0.5
	Beam	23.5	0.5	23.5	0.5

Table 2. Main parameters of the elasto-plastic material model.

Rebar	Yield strength (MPa)	Ultimate strength (MPa)	Elastic modulus (GPa)
ϕ10 (Diameter = 10 mm)	506.4	738.6	196.5
ϕ19 (Diameter = 19 mm)	431.7	734.4	193.8
ϕ25 (Diameter = 25 mm)	512.5	663.3	208.5

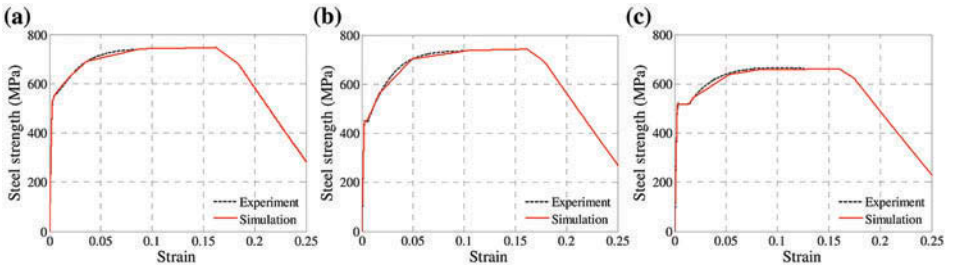

Figure 4. Comparison of steel stress–strain behavior between experiment and simulation: (a) ϕ10 steel rebar; (b) ϕ19 steel rebar; and (c) ϕ25 steel rebar.

parameters of this material model were defined based on the quasi-static testing results for each rebar size embedded in the test frames. The yield strengths and elastic modulus for the ϕ10, ϕ19, and ϕ25 steel reinforcing bars are summarized in Table 2. The strain corresponding to the ultimate strength was assumed to be approximately 15%. After the ultimate strength, the steel material models represented softening behavior until 25% strains. As shown in Figure 4, the selected material model was verified with the material tests for the ϕ10, ϕ19, and ϕ25 steel reinforcing bars.

3.2.3. *FRP Composite Material*

This study modeled the prefabricated FRP jackets on the first-story columns using the ORTHOTROPIC_ELASTIC (MAT002, referred to as "orthotropic material") model in LS-DYNA. This material model is characterized by elastic modulus (E), shear modulus (G), and Poisson's ratio (v) in terms of the three local principal axes (a, b, and c). Thus, the orthotropic material can simulate the directional characteristics of FRP materials [LSTC – Livermore Software Technology Corporation, 2013]. The main parameters (E_a, G_{ab}, and v_{ab}) of the orthotropic material in the hoop direction used in this study are 95.5 GPa, 4.5 GPa, and 0.28, respectively. The failure criterion was assigned 1.1% ultimate strain of the FRP material. Recent studies [Mutalib and Hao, 2010; Nam *et al.*, 2009; Youssf *et al.*, 2014] utilized the

orthotropic model to simulate and verify the FRP material behavior for FRP-strengthened RC structures. In particular, Youssf and ElGawady [2014] verified the material behavior of FRP-confined concrete by using the orthotropic model for the FRP materials, which indicates that the orthotropic material can predict the confining pressure provided by the FRP materials.

3.3. *Bond-Slip Modeling*

The bond-slip effects between steel reinforcing bars and concrete significantly affected the structural responses of RC structures [Spacone and Limkatanyu, 2000; Luccioni *et al.*, 2005; Bao and Li, 2010]. The non-ductile RC frame has short lap-splice reinforcing bars in the columns, a straight anchorage of positive (bottom) beam reinforcing bars, and no transverse reinforcement in the beam–column joint regions. Since such inadequate reinforcing details can lead to poor bonding conditions in RC structures, the bond-slip effects are critical to develop the as-built FE frame models. Several existing RC building structures were built with inadequate concrete cover using lower-quality concrete materials that were available at the time of construction; these factors often lead to corrosion of steel reinforcement. Reinforcement corrosion can result in a significant loss of bond strength between the surrounding concrete and the bar, decreasing the overall seismic performance of the structure [Deaton, 2013]. For RC structures, the effect of corrosion on the bond-slip behavior is typically critical after the onset of spalling in the concrete cover [Beeby, 1978]. The experimental results used to verify the FE frame model in the present work came from tests on non-damaged test frames performed within 18 months of construction. As such, steel corrosion would have no significant impact on bond-slip behavior. Therefore, the FE frame models presented here do not include the effect of steel corrosion on bond-slip behavior.

3.3.1. *One-Dimensional Slide Line Model*

A one-dimensional slide line model provided by LS-DYNA can transfer interfacial shear forces between the slave nodes of the reinforcing bar beam elements and the master nodes of the concrete solid elements. The interfacial forces are proportional to the slip displacement between the slave nodes and the master nodes. These one-dimensional slide line models can simulate the bond-slip effects by defining the bond shear modulus (G_s), maximum elastic slips (s_{max}), and the damage curve exponential coefficient (h_{dmg}), as given in Equation (3). The h_{dmg} decays the bond shear stress with the increment of plastic slip displacement (Δs_p), and D is the damage parameter, the sum of the absolute values of Δs_p ($D_{n+1} = D_n + \Delta s_p$, where n is an incremental step). As defined in Equation (3), the bond-slip behavior is assumed to be bilinear and the bond stress deterioration is initiated after reaching τ_{max} (= $G_s \cdot s$).

$$\tau = \begin{cases} G_s s, & s \le s_{\max} \\ \tau_{\max} e^{-h_{dmg} D}, & s > s_{\max} \end{cases} \tag{3}$$

Shi *et al.* [2008] modeled the bond-slip interface behavior between the beam elements and the surrounding concrete solid elements in an RC column using the one-dimensional slide line in LS-DYNA for blast loading. The FE column model with bond-slip effects shows better prediction of the blast responses than the numerical model calibrated by Woodson and Baylot [1999]. Researchers [Shi *et al.*, 2009] also modeled the bond-slip effects with the one-dimensional slide line model to simulate pullout responses in RC beam elements and verify the responses with experimental results. The bond-slip parameters in the one-

dimensional slide line model were calibrated based on the experimental results. The calibrated FE models demonstrated the pullout testing results. Additionally, to demonstrate the collapse scenarios of RC beam–column assemblies, Bao *et al.* [2008] developed FE models with the bond-slip effects. These bond-slip effects were also simulated with one-dimensional slide line models between beam longitudinal bars and the surrounding concrete in the panel zone. The FE models appropriately predict the collapse scenarios.

3.3.2. *Experimental Response for Bond-Slip*

A previous experimental study on a non-ductile RC test frame [Wright, 2015] demonstrated bond-slip behavior in column lap-splice and straight anchorage (positive beam reinforcing bars in beam–column joint areas) using test results obtained from a full-scale dynamic experiment. The bond-slip behavior in lap-splice and joint areas was identified by comparing the measured hinge rotations in beams or columns to reinforcing bar strain in those areas under dynamic loads. The relationship between the peak hinge rotations and the corresponding bar strains is summarized in Figures 5 and 6, respectively, for each loading sequence for the as-built and retrofitted test frames. Figure 5a shows the relationship between peak column hinge rotations in first-story column bases and the corresponding bar strains for each loading sequence. If no bond-slip failure in the lap-splice regions was observed, then the peak column hinge rotations should continuously increase in accordance with the shaker force increment. Furthermore, the bar strains should also keep increasing prior to the yielding of steel reinforcing bars. However, it was observed in the experiment that the lap-splice bar strain decreased after reaching the peak bar strain, which occurred before the yielding of steel reinforcing bars. This phenomenon is believed to have occurred due to concrete cracks in the lap-splice regions (e.g. splitting cracks along the column reinforcing bars and shear cracks), which contributed to the losses of the interface forces between the lap-splice bars and the surrounding concrete. Figure 5b demonstrates the pullout behavior in the positive beam reinforcing bars in the first-story exterior beam–column joints. However, the maximum bar strains in the negative beam reinforcement are continuously increased due to 180° anchorage hooks. More detailed test results of the bond-slip behavior for the as-built test frame can be found in Wright [2015].

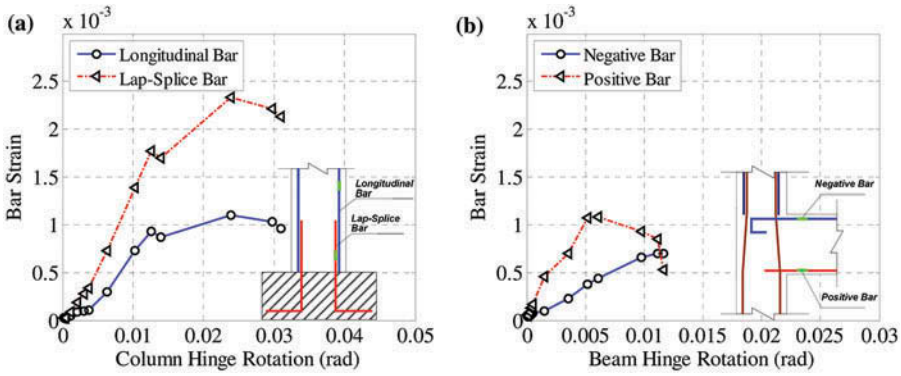

Figure 5. Relationships between peak hinge rotations and bar strains for the as-built test frame: (a) first-story column; and (b) first-story exterior beam–column joint.

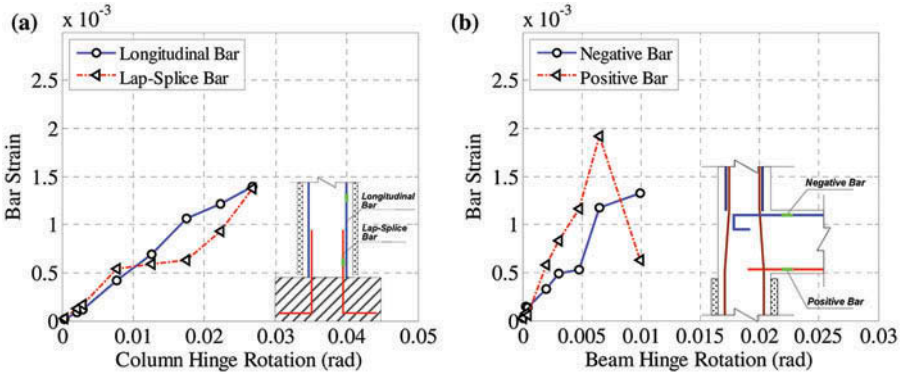

Figure 6. Relationships between peak hinge rotations and bar strains for the retrofitted test frame: (a) first-story column; and (b) first-story exterior beam–column joint.

Through the full-scale dynamic testing of the retrofitted test frame, the bond-slip responses were also observed using the same approach as the as-built test frame. Figure 6a proves that the installation of the FRP column jacket system in first-story columns can help delay the bond-slips of the column lap-splice bars since the maximum bar strains keep increasing with the peak column hinge rotations. This is due to the additional confining pressures provided by the FRP jacket system. As shown in Figure 6b, strain readings in bottom reinforcing bars taken near an exterior beam–column joint indicated a decrease in bar strains after they reached a maximum value but before yielding in the bar. This decrease indicates a pullout failure in the exterior beam–column joints. Based on these observations in the full-scale dynamic tests, this study determined the bonding conditions and failure modes for the locations where the bond-slip effects were significantly affected.

3.3.3. *Numerical Bond-Slip Model*

This study characterized the bond-slip performance in the FE frame models using the CEB-FIP MODEL CODE [1990]. The model code defines the bond stress–slip relationship depending on failure modes (e.g. splitting (lap-splice) and pullout failure modes) and bonding conditions (e.g. good and poor conditions). The bonding conditions can be determined by confining pressures regarding the concrete cover and the reinforcement detailing, such as column lap-splice length, transverse reinforcing details, and anchorage details in beam–column joints. Figure 7 compares the bond stress–slip relationships between the model code and the one-dimensional slide line model in LS-DYNA. The bond stress deterioration was captured using the h_{dmg} parameter discussed in Section 3.3.1. The values of h_{dmg} in terms of the failure modes and bonding conditions were found through calibrating the residual bond stresses of the model code with those of the one-dimensional slide line model. The values of h_{dmg} for good and poor bonding conditions in the lap-splice failure are 0.25 and 0.065, respectively, and the value of h_{dmg} for good and poor bonding conditions in the pullout failure is 0.01.

Figure 8 shows the representative bond-slip modeling used in the FE frame models with respect to the failure modes and bonding conditions determined based on the experimental studies [Wright, 2015; Shin *et al.*, 2016]. Figure 9 indicates the locations where bond-slip effects are thought to occur. As shown in Figure 8a and b, the bond-slip models

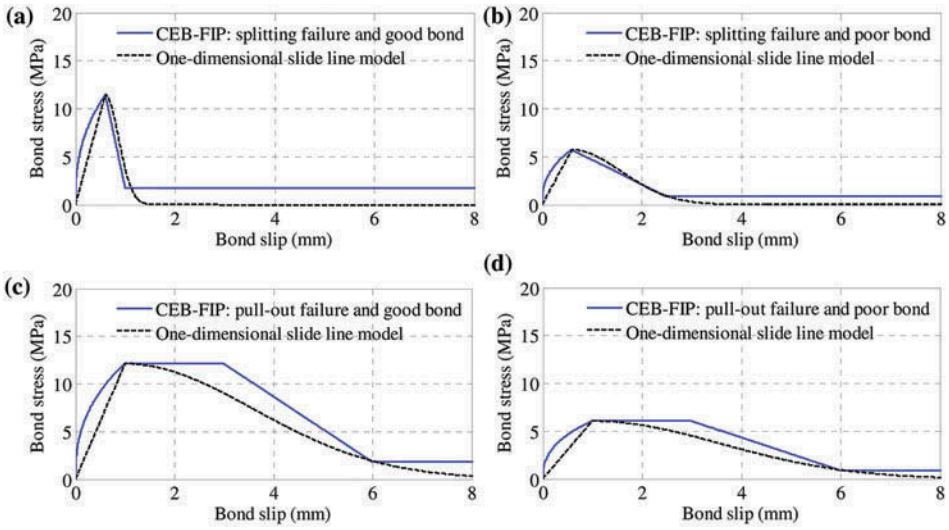

Figure 7. Comparisons of bond stress–slip relations between the CEB-FIP Model Code and the one-dimensional slide line model in LS-DYNA: (a) splitting failure and poor bond; (b) splitting failure and good bond; (c) pullout failure and good bond; and (d) pullout failure and poor bond.

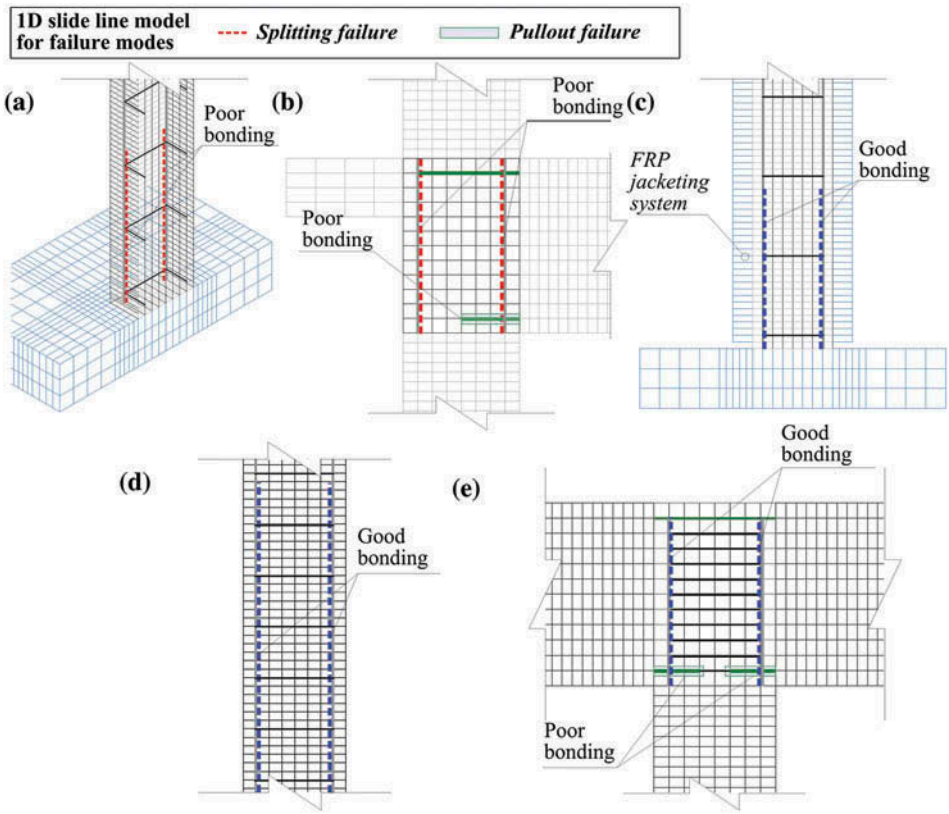

Figure 8. Examples of bond-slip modeling for failure modes and bonding conditions in LS-DYNA: (a) first-story as-built column; (b) first-story exterior beam–column joint; (c) first-story retrofitted column; (d) second-story column; and (e) second-story interior beam–column joint.

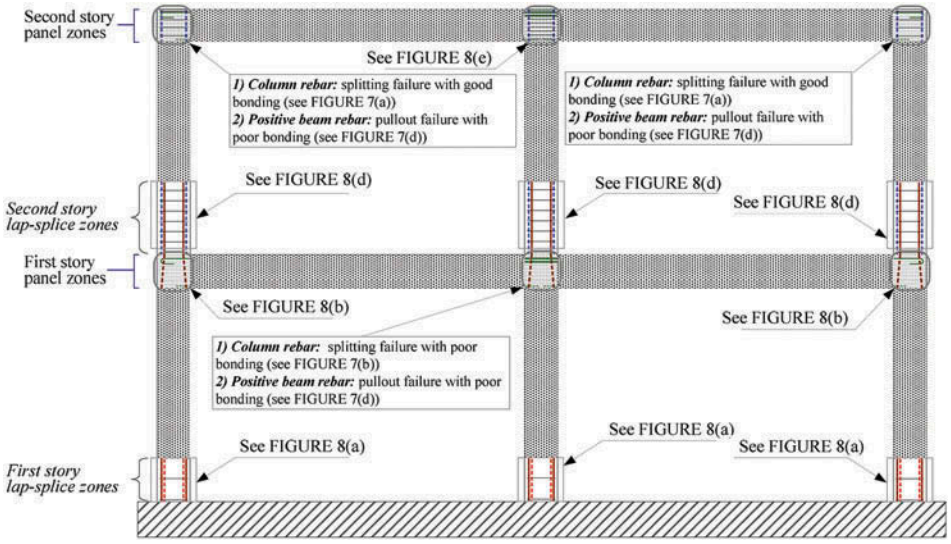

Figure 9. Bond-slip model locations for the as-built FE frame model.

in first-story as-built columns and positive beam reinforcing bars were defined based on the full-scale dynamic testing results (see Figures 5 and 6). The test results also demonstrated that the installation of FRP column jackets system improved the bonding condition of the column lap-splice bars (see Figure 6a). Thus, as shown in Figure 8c, the bond-slip effects in the column lap-splice regions of the retrofitted FE frame model were simulated with the bond stress–slip response determined by the splitting failure mode and the good bonding condition. The second-story columns have longer lap-splice length and smaller spacing of column ties with seismic detailing (i.e. 135° specified angle), which was to transfer the vibration loads from the second story to the first story without an unexpected failure during the experiment [Shin *et al.*, 2016]. Thus, the bond-slip behavior of lap-splice zones in second-story columns was modeled with a splitting failure mode and good bonding condition, as given in Figure 8d.

Since no instrumentation was installed inside the panel zones and transverse beams supporting slabs inhibited a visible inspection on the surface of panel zones, this study assumed failure modes and bonding conditions between the column reinforcing bars and the surrounding concretes inside the panel zones. Past experimental studies [Akguzel, 2011; Engindeniz, 2008; Park and Mosalam, 2012] on non-ductile beam–column joints constructed prior to the 1970s, which have no transverse reinforcing bars inside the panel zones, detected visible damage on the surface of panel zones, such as shear cracks and splitting cracks along the column reinforcing bars in the panel zones. In particular, the splitting cracks resulted in confinement losses between the column reinforcing bars and the surrounding concrete, and these confinement losses can produce significant bond-slip effects. The second-story panel zones, as given in Figures 8e and 9, have transverse beam reinforcing bars, similar to current seismic design requirements. These can minimize the bond-slip effects of the column reinforcing bars inside the panel zones. Therefore, this study assumed bond-slip conditions for the column reinforcing bars in the panel zones as the splitting failure mode with poor bonding condition in the first story (see Figure 8b) and the splitting failure mode with good

bonding condition in the second story (see Figure 8e). This study utilized the FE frame models with all possible bond-slip effects for the verification with the experimental responses.

4. Verification of FE Numerical Frame Models

4.1. *Shaker Forces*

During full-scale dynamic testing, test frames were vibrated by shaker forces induced from a hydraulic linear shaker on the roof. The linear shaker generated two different types of excitations: seismic and sine vibrations. The amplitudes of the shaker force in each input excitation were scaled by the increase in the target displacement of the linear shaker [Shin *et al.*, 2016]. To verify the elastic and inelastic responses, this study selected two different types of loading scenarios for each FE frame model: the 1940 El Centro (EC) earthquake with 203 mm (8 inch) target displacement (EC 8) and double sine pulse (DSP) vibration with 660 mm (26 inch) target displacement (DSP 26 – ultimate loading scenario) for the as-built FE frame model, and EC 8 and DSP vibration with 508 mm (20 inch) target displacement (DSP 20 – ultimate loading scenario) for the retrofitted FE frame model. The full-scale dynamic testing for the as-built test frame was performed under various loading sequences. Among them, DSP 26 was selected as the ultimate loading scenario for the as-built FE frame model because it induced significant bond-slip effects in the column lap-splice and panel zones during the full-scale dynamic testing for the as-built test frame [Wright, 2015]. For the retrofitted FE frame model, DSP 20 was chosen as the ultimate loading scenario, which initiated pullout failure between the bottom beam reinforcing bars and the surrounding concrete. The seismic and sine vibrations were applied to the rigid plates of the FE frame models as shaker forces. These shaker forces, $F(t)$, were computed as given in Equation (4), where m_s is the mass of the linear shaker and $\ddot{x}_s(t)$ is the absolute acceleration of the shaker. This acceleration data was measured by an accelerometer, mounted directly to the shaker mass in the in-plane direction. To eliminate the noises of the measured acceleration, the acceleration data were filtered. As an example, the filtered and measured shaker accelerations for the as-built test frame are plotted in Figure 10, with EC 8 in Figure 10a and DSP 26 in Figure 10b.

$$F(t) = -m_s\ddot{x}_s(t) \tag{4}$$

4.2. *As-Built FE Frame Model*

Figure 11 compares the displacement-time history responses between the experimental and simulated results in the first and second stories under the EC 8 loading. As observed in the full-scale dynamic tests, this loading scenario did not induce any significant damage on the structure [Wright, 2015]. Thus, the bond-slip effects were expected to be marginal in this loading scenario. This loading scenario was taken into account to verify the dynamic behavior within an elastic range. The as-built FE frame model predicted the experimental results in terms of the response period over the full range of time. The maximum absolute story displacement of the experimental and simulated responses at t_1 (= 1.33 s) and t_2 (= 4.19 s) is plotted in Figure 12a and b, where t_1 and t_2 denote the time at which the first and second stories have the maximum displacements in the displacement-time history responses obtained from the experiment, respectively. The FE frame model slightly underestimates the maximum displacement at t_1 by approximately 10.0% (see Figure 12a), and it overestimates the maximum displacement at t_2 by

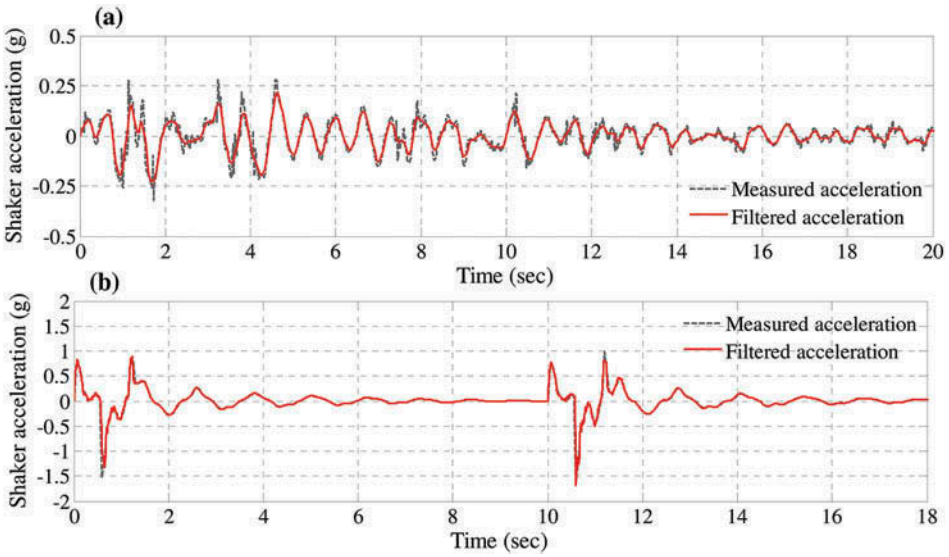

Figure 10. Measured and filtered shaker accelerations for the as-built FE frame model: (a) seismic excitation, 1940 El Centro earthquake (EC 8); and (b) double sine pulses (DSP 26).

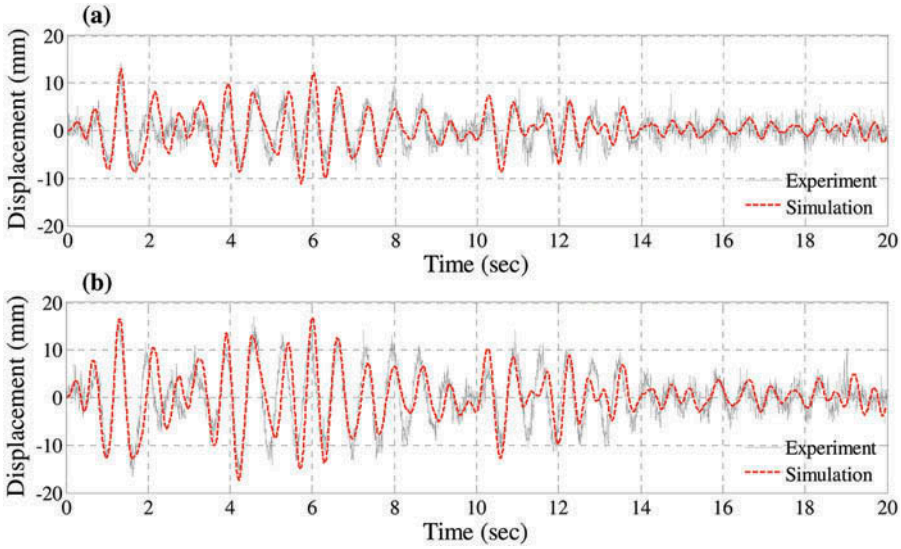

Figure 11. Comparison of time-history responses for the as-built FE frame model between experimental and simulated responses: (a) first story; (b) second story.

approximately 9.0% (see Figure 12b). Figure 13 shows the peak inter-story drift ratios obtained from the experiment and simulation. The peak inter-story drift ratios of the simulated results are plotted at the time when the maximum drift response occurs for each story level. While the peak inter-story drift ratio in the first story is approximately 4.0% lower than the experimental results, the peak inter-story drift ratio in the second story is approximately 10.0% higher than the experimental results.

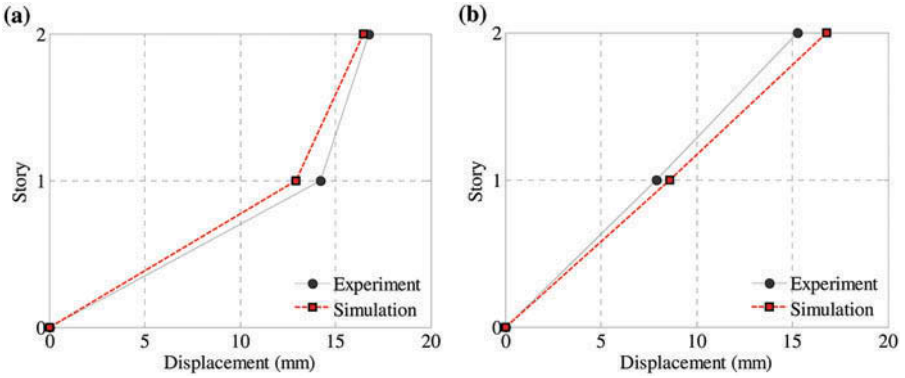

Figure 12. Comparison of story displacements for the as-built FE frame model between the experimental and simulated responses: (a) t_1 time step; (b) t_2 time step.

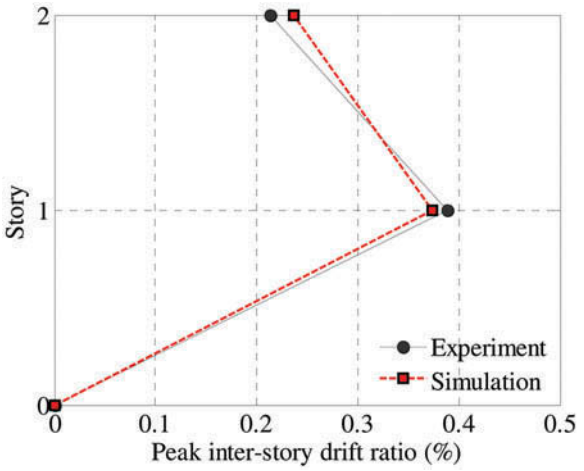

Figure 13. Comparison of peak inter-story drift ratios for the as-built FE frame model between the experimental and simulated responses under EC 8.

Figure 14 illustrates the experimental and simulated time history responses in the first and second stories under the DSP 26 loading. Overall, the simulated and experimental results are in good agreement in terms of the response periods. The maximum absolute story displacements for the first and second stories were found at t_1 = 11.4 and t_2 = 11.5 s, respectively. The story displacements at t_1 and t_2 are plotted in Figure 15a and b, respectively. The maximum simulation variation for the story displacements of the FE frame model at t_1 and t_2 is approximately 7.0% and 8.0%, respectively. Figure 16 compares the peak inter-story drift ratios between the experiment and the simulation. The peak inter-story drift ratio in the second story was overestimated by approximately 9.0%.

Overall, the simulation variation was estimated below 10.0%. This variation was attributed to some of the assumptions made in the FE frame model. First, while additional masses, placed on the first and second floors using steel rails for live loads, slid along the slab slightly during the

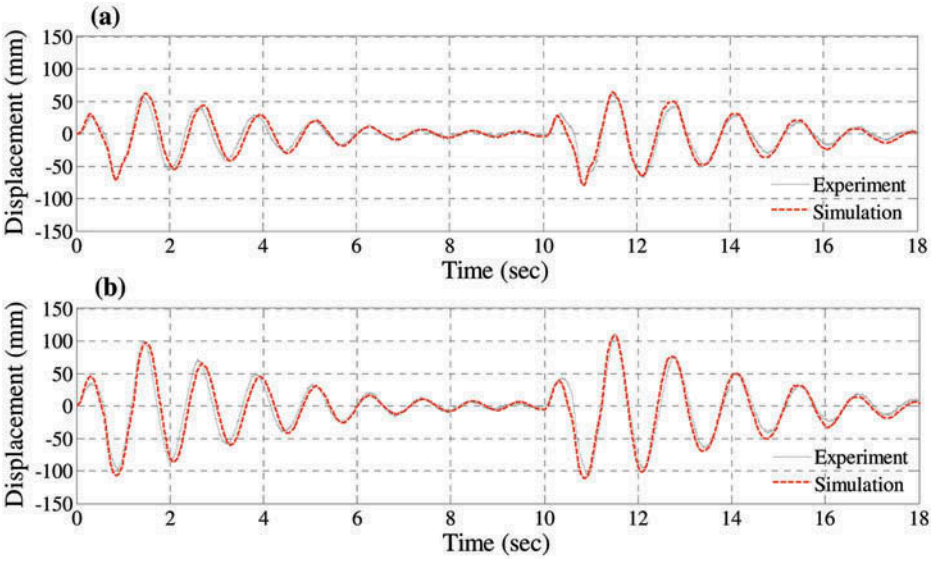

Figure 14. Comparison of time-history responses for the as-built FE frame model between experimental and simulated responses under DSP 26: (a) first story; (b) second story.

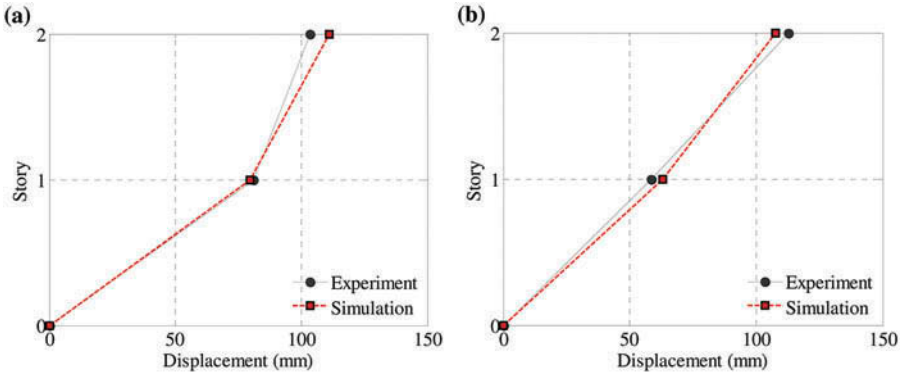

Figure 15. Comparison of story displacements for the as-built FE frame model between experimental and simulated responses under DSP 26: (a) t_1 time step; (b) t_2 time step.

dynamic tests, the masses in the FE frame model were modeled to be fixed (fixed mass condition). Second, the test frame was vibrated under sequential loading scenarios. However, the FE frame model was assumed to be non-damaged under the selected loading scenarios. Finally, to reduce the computational time of the FE frame model, slab, transverse beam, and foundation elements (noncritical elements), where no significant damage was found from the full-scale dynamic testing, were simplified with the effective stiffness. These assumptions led to the slight simulation variation between the experimental and simulated responses. Nevertheless, the FE frame model is able to capture the dynamic responses in terms of the response periods, story displacements, and inter-story drift ratios. In particular, the full-scale dynamic tests demonstrated that the dynamic responses of the as-built test frame were significantly affected

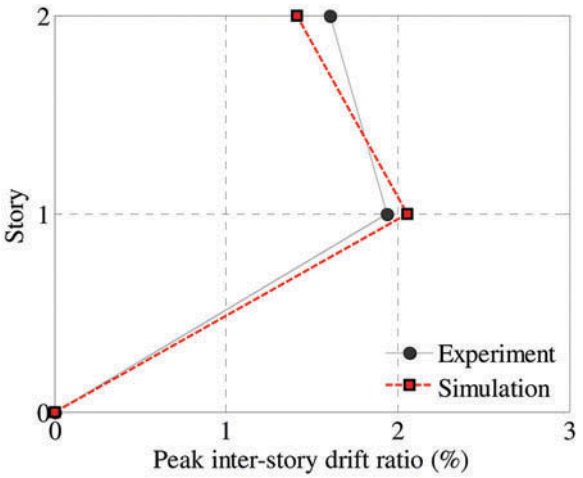

Figure 16. Comparison of peak inter-story drift ratio for the as-built FE frame model between experimental and simulated responses under DSP 26.

by bond-slip behavior in the first-story column bases and exterior beam–column joints under the DSP 26 loading. Simulations using the bond-slip modeling procedure described here resulted in maximum displacements in the FE frame model within 10.0% of those observed during the experimental investigation under DSP 26 loading.

4.3. *Retrofitted FE Frame Model*

To validate the dynamic responses of the retrofitted FE frame model, the same approach used in the verification works of the as-built FE frame model was adopted. Experimental responses of the retrofitted test frame were gathered from the full-scale dynamic test [Shin *et al.*, 2016]. Figure 17 shows the experimental and simulated displacement-time history responses of the retrofitted frame under EC 8 loading. As illustrated in Figure 17a and b, the retrofitted FE frame model captured the experimental results in terms of the response period in entire time steps. The maximum absolute story displacements at t_1 = 1.06 and t_2 = 4.40 s are plotted in Figure 18a and b, respectively. The first-story displacement at t_1 was underestimated within approximately 9.8% simulation variation, and the FE frame model underestimated the first-story displacement at t_2 by approximately 6.7%. Figure 19 compares the peak inter-story drift ratios of the retrofitted frame between experiment and simulation. The maximum variation for the inter-story drift ratio was estimated within 10.0%.

Figure 20 illustrates the displacement-time history responses under DSP 20, an ultimate loading scenario for the retrofitted test frame. The FE frame model can capture the response periods before the beginning of a second loading cycle. However, the response periods were slightly overestimated during the second loading cycle in DSP 20. This is thought to be due to the structural damage accumulations induced by the first loading cycle in DSP 20. Figure 21 compares the experimental and simulated story displacements at t_1 = 6.18 and t_2 = 6.23 s. The FE frame model underestimated the maximum story displacement by approximately 5.5% at t_1, whereas it overestimated the maximum story displacement by approximately 4.8% at t_2. Figure 22 shows the experimental and simulated peak inter-story drift ratios. The peak inter-

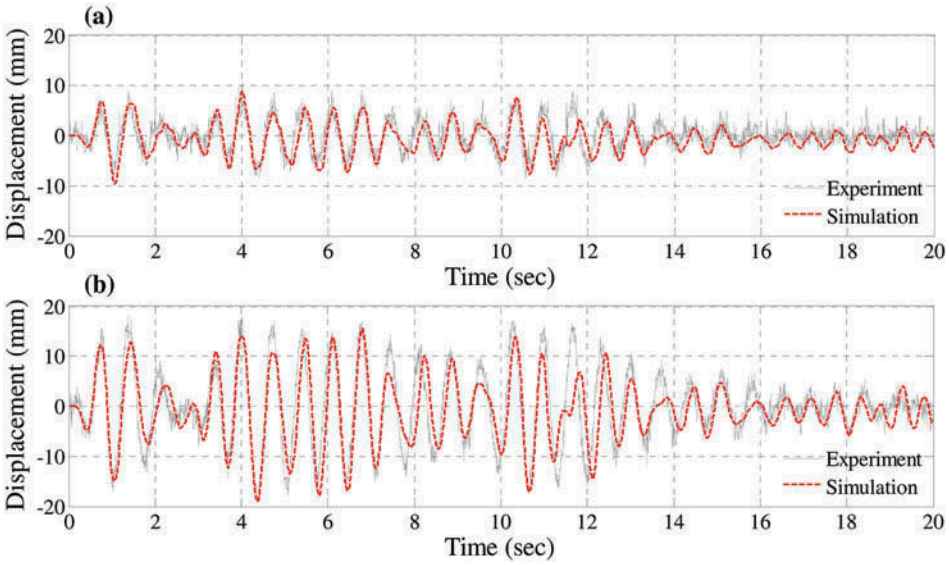

Figure 17. Comparison of time-history responses for the retrofitted FE frame model between the experimental and simulated responses under EC 8: (a) first story; (b) second story.

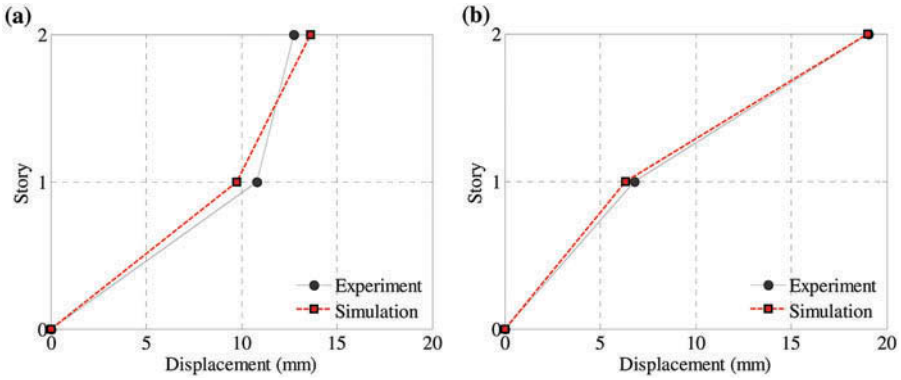

Figure 18. Comparison of story displacements for the retrofitted FE frame model between experimental and simulated responses under EC 8: (a) t_1 time step; (b) t_2 time step.

story drift ratio was slightly underestimated by approximately 11.5% compared with the experimental results in the second story.

4.4. *Damage*

Figure 23 compares the damage at the first-story column bases between the experimental and simulated results. Figure 23a shows the locations of damage observed from the full-scale dynamic testing for the as-built and retrofitted test frames. As shown in Figure 23b, diagonal cracks at the lap-splice zone of the first-story column were detected in the as-built test frame. For the retrofitted test frame, a crack at the edge of the column base was observed as shown

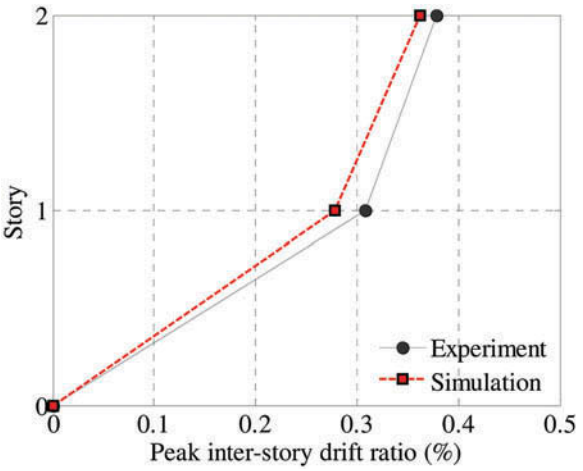

Figure 19. Comparison of peak inter-story drift ratio for the retrofitted FE frame model between the experimental and simulated responses under EC 8.

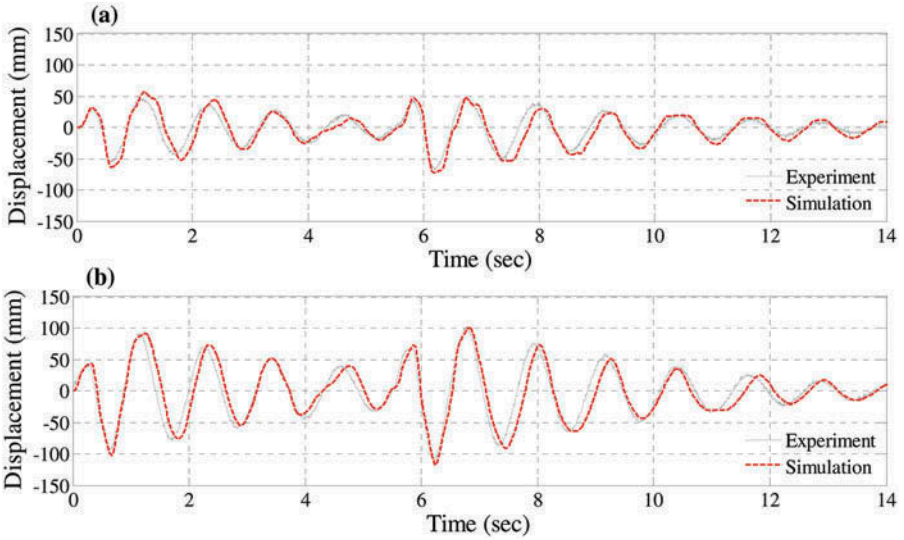

Figure 20. Comparison of time-history responses for the retrofitted FE frame model between the experimental and simulated responses under DSP 20: (a) first story; (b) second story.

in Figure 23c. Figure 23d and 23e shows the damage on the first-story column lap-splice zones in the as-built and retrofitted FE frame models using effective plastic strains. The color fringe level for the effective plastic strains of concrete materials is scaled from 0 to 2. The value of 2 in the fringe level represents concrete cracking under tension and concrete crushing under compression [Lin *et al.*, 2014]. As shown in Figure 23d, the as-built FE frame model exhibits diagonal cracks at the first-story column lap-splice zone, similar to what was observed during the full-scale dynamic experiments. The retrofitted FE frame model simulates the concrete crack at a gap between the FRP column jacketing system and

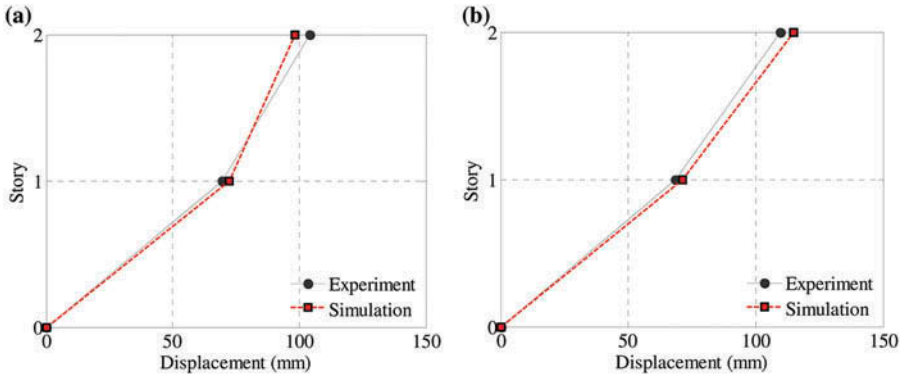

Figure 21. Comparison of story displacements for the retrofitted FE frame model between the experimental and simulated responses under DSP 20: (a) t_1 time step; (b) t_2 time step.

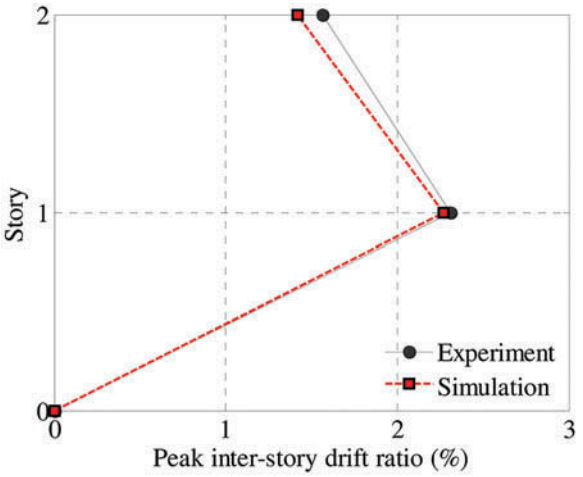

Figure 22. Comparison of peak inter-story drift ratio for the retrofitted FE frame model between the experimental and simulated responses under DSP 20.

the foundation (Figure 23e), similar to the observed damage from the full-scale dynamic testing.

4.5. *Effects on Bond-Slip Modeling*

To investigate the necessity of including bond-slip performance in simulations, the dynamic responses of FE frame models described in the previous sections (referred to as "True bond-slip") were compared to those of FE frame models with two different other bond-slip conditions: (1) true bond-slip effects with all good bonding conditions (referred to as "Good bond-slip"), and (2) no bond-slip effects (perfectly bonded between reinforcing bars and surrounding concrete, referred to as "No bond-slip"). The true bond-slip models have combinations of poor and good bonding conditions based on reinforcing detailing in the column lap-splice and panel zones as described above. The good bond-slip

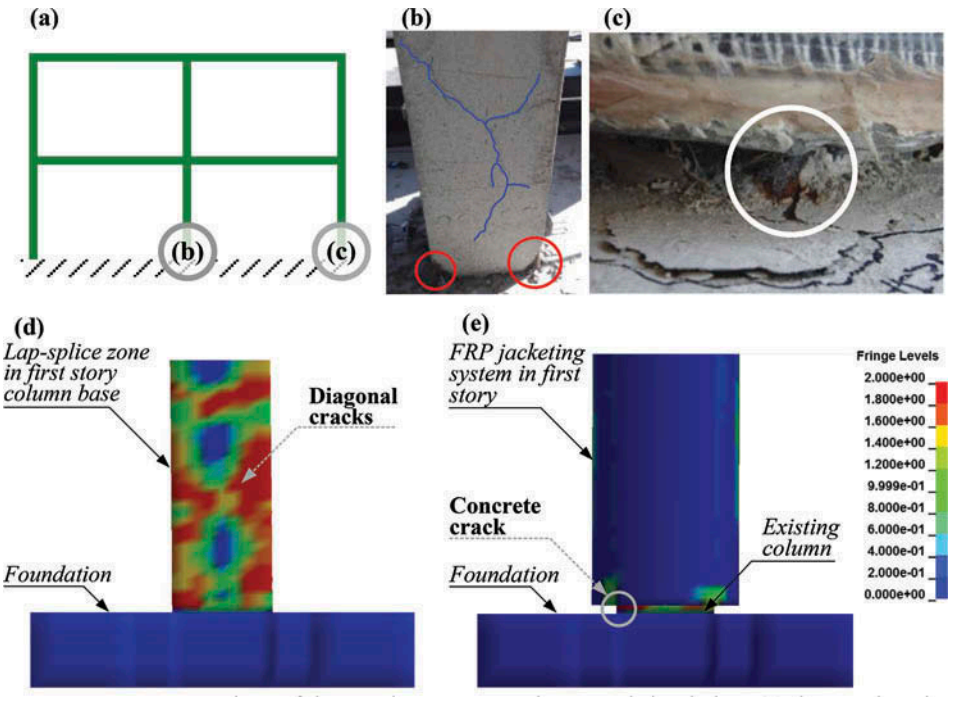

Figure 23. Comparison of damage between experiment and simulation: (a) damage location of the as-built and retrofitted test frames; (b) damage observed on the as-built test frame [Wright, 2015]; (c) damage observed on the retrofitted test frame [Shin *et al*., 2016]; (d) damage suggested by the as-built FE frame model; (e) damage suggested by the retrofitted FE frame model.

models were modeled with the good bonding condition in all possible areas where bond-slip effects occur regardless of the reinforcing detailing. Additionally, the no bond-slip models deactivated the one-dimensional slide line models in the column lap-splice and panel zones and the beam elements were merged with the nodes of concrete solid elements (perfect bonding between the reinforcing bars and the concrete material). Those effects were estimated under each ultimate loading scenario (DSP 26 for the as-built FE frame model and DSP 20 for the retrofitted FE frame model) because the bond-slip effects are marginal in elastic range behavior due to negligible slip displacements between the reinforcing bars and the surrounding concrete.

Figure 24 shows the roof time-history responses of the true bond-slip, good bond-slip, and no bond-slip models. Figure 25 compares the maximum simulated responses of the true bond-slip models to those of the no bond-slip models for the first and second sine vibrations of simulations. For the as-built frame models, as shown in Figure 24a, the overall responses of the no bond-slip model are significantly less than those of the true bond-slip model. The maximum response of the no bond-slip model in the first sine vibration is approximately 39.0% lower than that of the true bond-slip model (see Figure 25). The main reason for this significant difference is that models using no bond-slip effects exhibit perfect bond between the reinforcing bars and the surrounding concrete in the lap-splices and panel zones, which greatly exaggerates the overall stiffness of the area.

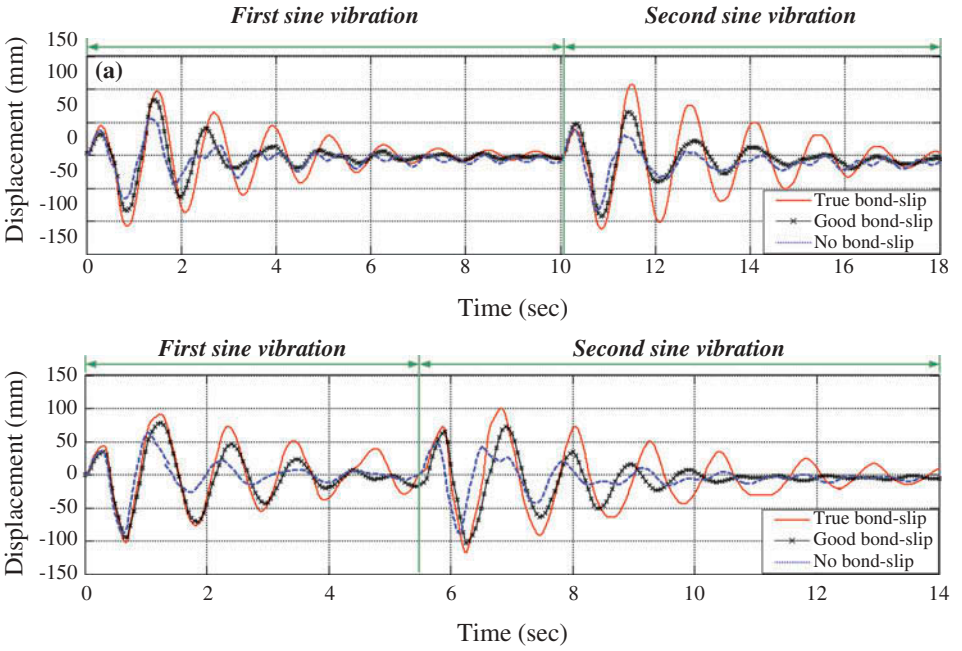

Figure 24. Roof time-history responses of the true bond-slip, good bond-slip, and no bond-slip models: (a) as-built FE frame model; and (b) retrofitted FE frame model.

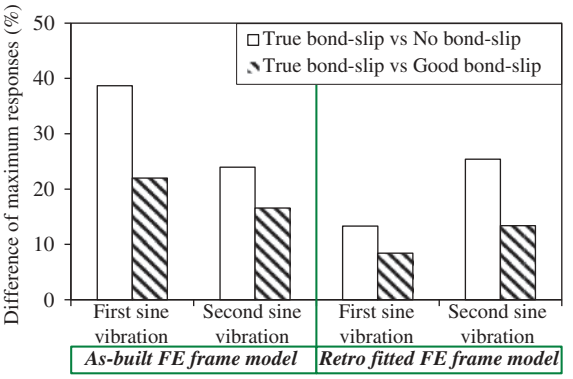

Figure 25. Comparison of maximum responses for the first and second sine vibrations.

The dynamic responses of the good bond-slip model are also less than those of the true bond-slip model. The maximum differences between the true bond-slip and good bond-slip models for the first and second sine vibrations are approximately 22.0% and 17.0%, respectively (see Figure 25). The good bond-slip model was modeled with a good bonding condition in poor bonding zones, such as first-story lap-splice and panel zones, and this inappropriate bonding condition resulted in higher bonding stiffness and stresses between the reinforcing bars and the surrounding concrete in the poor bonding zones.

Compared with the true bond-slip model for the retrofitted frame, Figure 24b shows that the overall responses of the no bond-slip and good bond-slip models are slightly less. In particular, during the first sine vibration of the simulations, the maximum responses of the no bond-slip and good bond-slip models are approximately 13.0% and 8.0% lower than those of the true bond-slip model, respectively. These slight differences are due to the effectiveness of the FRP column jacket system in the first-story columns, which delayed bond-slip effects by minimizing concrete damage within the first-story lap-splice and panel zones in the early steps of the simulations. In other words, during the early run-time, the effects of bond-slip models for the retrofitted FE frame models are marginal. However, after the loading step is increased, the dynamic responses of the no bond-slip model were significantly less than those of the true bond-slip model by approximately 25.0%. This is because the assumption of no-bond slip, in which the reinforcing bars were perfectly bonded with the surrounding concrete in the lap-splice and panel zones, exaggerated bonding stiffness in all possible bonding zones. Similar to the no bond-slip model, Figure 25 illustrates that the good bond-slip model has a higher difference with the true bond-slip model during the second sine vibration of the simulation than during the first sine vibration because of the bond-slip model with inappropriate bonding conditions in the first-story panel zones. This modeling assumption failed to predict reasonable bond-slip behavior during the second sine vibration of the simulation.

5. Summary and Conclusion

The present work developed numerical FE models of full-scale as-built (non-ductile) and retrofitted test frames subjected to dynamic loads using LS-DYNA [LSTC – Livermore Software Technology Corporation, 2013]. Past experimental studies [Wright, 2015; Shin *et al.*, 2016] demonstrated that the bond-slip effects significantly affected the soft-story failure mechanism of the as-built test frame. Based on these full-scale dynamic tests, this study determined the bonding performance conditions and the failure modes for the locations where the bond-slip effects were detected. The bond-slip behavior was modeled using one-dimensional slide line models between the reinforcing bars and the surrounding concrete. The developed FE frame models were simulated under seismic and sine vibrations (ultimate loading scenarios) measured from the full-scale dynamic tests. Additionally, the effects on various bond-slip models were estimated under the ultimate loading scenarios. Based on this investigation, the following conclusions can be drawn.

(1) The developed FE frame models were validated with past experimental responses under the seismic and sine vibrations in terms of story displacements and inter-story drifts within 12.0% simulation variation. This slight simulation variation for the ultimate loading scenarios appropriately verified the experiment-based bond-slip modeling process utilized in this study. The simulation variation was attributed to the following modeling assumptions: (1) fixed mass conditions; (2) non-damaged conditions; (3) effective stiffness using an elastic material model; and (4) assumed frictional coefficients in the surface layers.
(2) By comparing the roof displacement time-histories of true bond-slip models to those of good bond-slip and no bond-slip models, the effects on bond-slip modeling were

estimated. The dynamic responses of no bond-slip and good bond-slip models were less than those of the true bond-slip models. This is because inappropriate bond-slip models produced higher bonding properties between the beam elements and the surrounding concrete solid elements in the lap-splice and panel zones, where the bond-slip effects occur. These bonding models affected the underestimation of the dynamic responses. Therefore, to capture reasonable simulations for the FE frame models, appropriate bond-slip modeling in the possible bonding zones is needed.

Acknowledgments

This support is gratefully acknowledged. Any opinions, findings, conclusions, or recommendations are those of the authors and do not necessarily reflect the views of other organizations.

Funding

This work was supported by the Division of Civil, Mechanical and Manufacturing Innovation [CMMI-1041607].

References

ACI Committee – American Concrete Institute, ACI 318-63. [1963] *Building Code Requirements for Reinforced Concrete*, American Concrete Institute, Detroit, Michigan.

Akguzel, U. [2011] "Seismic performance of FRP retrofitted exterior RC beam-column joints under varying axial and bidirectional loading," Ph.D. thesis, Department of Civil Engineering, University of Canterbury, Christchurch, New Zealand.

ASCE – American Society of Civil Engineers, ASCE/SEI 41-13. [2014] *Seismic Evaluation and Retrofit of Existing Buildings*, American Society of Civil Engineers, Reston, Virginia.

Aschheim, M., Gülkan, P., Sezen, H., Bruneau, M., Elnashai, A. S., Halling, M., Love, J. and Rahnama, M. [2000] "Performance of buildings," *Earthquake Spectra* **16**(S1), 237–279.

Bao, Y., Kunnath, S.K., El-Tawil, S., & Lew, H.S. [2008]. Macromodel-based simulation of progressive collapse: RC frame structures. *Journal of Structural Engineering* **134**(7): 1079–91.

Bao, X. and Li, B. [2010] "Residual strength of blast damaged reinforced concrete columns," *International Journal of Impact Engineering* **37**(3), 295–308.

Beeby, A. W. [1978] "Corrosion of reinforcing steel in concrete and its relation to cracking," *Structural Engineer* **56**, 3.

Bracci, J. M., Reinhom, A. M. and Mander, J. B. [1995] "Seismic resistance of reinforced concrete frame structures designed for gravity loads: performance of structural system," *ACI Structural Journal* **92**(5), 597–609.

Broadhouse, B. J. [1986] *DRASTIC: A Compute Code for Dynamic Analysis of Stress Transients in Reinforced Concrete*, Safety and Engineering Science Division, AEE, Winfrith.

CEB-FIP MODEL CODE [1990]. "Model code for concrete structures," In: Comité Euro-International du Béton. Secretariat permanent. Case Postale 88, CH-1015 Lausanne, Switzerland.

Crawford, J. E., Wu, Y., Choi, H., Magallanes, J. M. and Lan, S. [2012] "Use and validation of the release III K&C concrete material model in LSDYNA," TR-11-36.6 Technical report, Karagozian & Case, Glendale, California.

Crawford, J. E., Wu, Y., Magallanes, J. M. and Choi, H. J. [2013] "The importance of shear-dilatancy behaviors in RC columns," *International Journal of Protective Structures* **4**(3), 341–377.

Davidson, J. [2008] "Advanced computational dynamics simulation of protective structures research," Technical Report No. AFRL-RX-TY-TR-2008-4610, Auburn University, Auburn, Ala.

Deaton, J. B. [2013] "Nonlinear finite element analysis of reinforced concrete exterior beam-column joints with nonseismic detailing," Ph.D. thesis, School of Civil and Environmental Engineering, Georgia Institute of Technology, Atlanta, Georgia.

El-Attar, A. G., White, R. N. and Gergely, P. [1997] "Behavior of gravity load designed reinforced concrete buildings subjected to earthquake," *ACI Structural Journal* **94**(2), 133–145.

ElGawady, M., Endeshaw, M., McLean, D. and Sack, R. [2010] "Retrofitting of rectangular columns with deficient lap splices," *Journal of Composites for Construction* **14**(1), 22–35.

Engindeniz, M. [2008] "Repair and strengthening of pre-1970 reinforced concrete corner beam-column joints using CFRP composites," Ph.D. thesis, School of Civil and Environmental Engineering, Georgia Institute of Technology, Atlanta, Georgia.

FEMA – Federal Emergency Management Agency, FEMA 547. [2006] *Techniques for the Seismic Rehabilitation of Existing Buildings*, Federal Emergency Management Agency, Washington D.C.

Haroun, M. A., Mossalam, A. S., Feng, Q. and Elsanadedy, H. M. [2003] "Experimental investigation of seismic repair and retrofit of bridge columns by composite jackets," *Journal of Reinforced Plastics and Composites* **22**(14), 1243–1268.

Hu, H. T., Huang, C. S., Wu, M. H. and Wu, Y. M. [2003] "Nonlinear analysis of axially loaded concrete-filled tube columns with confinement effect," *Journal of Structural Engineering* **129**(10), 1322–1329.

Kwon, M. and Spacone, E. [2002] "Three-dimensional finite element analyses of reinforced concrete columns," *Computers & Structures* **80**(2), 199–212.

Lee, D. and Shin, A. H. C. [2016] "Finite element study on the impact responses of concrete masonry unit walls strengthened with fiber-reinforced polymer composite materials," *Composite Structures* **154**, 256–268.

Lin, X., Zhang, Y. X. and Hazell, P. J. [2014] "Modelling the response of reinforced concrete panels under blast loading," *Materials & Design* **56**, 620–628.

LSTC – Livermore Software Technology Corporation. [2013] *LS-DYNA Keyword User's Manual Version 971/R7.0*. Livermore Software Technology Corporation, CA.

Luccioni, B. M., López, D. E. and Danesi, R. F. [2005] "Bond-slip in reinforced concrete elements," *Journal of Structural Engineering* **131**(11), 1690–1698.

Malvar, L. J., Crawford, J. E., Wesevich, J. W. and Simons, D. [1997] "A plasticity concrete material model for DYNA3D," *International Journal of Impact Engineering* **19**(9), 847–873.

Moradi, L. G. [2007] "Resistance of membrane retrofit concrete masonry walls to lateral pressure," Ph.D, Dissertation, Univ. of Alabama at Birmingham, Birmingham, Ala.

Mutalib, A. A. and Hao, H. [2010] "Numerical analysis of FRP-composite-strengthened RC panels with anchorages against blast loads," *Journal of Performance of Constructed Facilities* **25**(5), 360–372.

Nam, J. W., Kim, H. J., Kim, S. B., Kim, J. H. and Byun, K. J. [2009] "Analytical study of finite element models for FRP retrofitted concrete structure under blast loads," *International Journal of Damage Mechanics* **18**(5), 461–490.

NEES@UCLA. [2015] *Network for Earthquake Engineering Simulation at the University of California, Los Angeles*, University of California, Los Angeles, Los Angeles, California. http://nees.ucla.edu.

Park, S. and Mosalam, K. M. [2012] "Experimental and analytical studies on old reinforced concrete buildings with seismically vulnerable beam-column joints," PEER Report 2012/03, Pacific Earthquake Engineering Research Center, University of California, Berkeley, Berkeley, California.

Priestley, M. J. N. [1997] "Displacement-based seismic assessment of reinforced concrete buildings," *Journal Earthquake Engineering* **1**(1), 157–192.

Sause, R., Harries, K. A., Walkup, S. L., Pessiki, S. and Ricles, J. M. [2004] "Flexural behavior of concrete columns retrofitted with carbon fiber-reinforced polymer jackets," *ACI Structural Journal* **101**(5), 708–716.

Schwer, L. E. and Murray, Y. D. [1994] "A three-invariant smooth cap model with mixed hardening," *International Journal for Numerical and Analytical Methods in Geomechanics* **18**(10), 657–688.

Seible, F., Priestley, M. J. N., Hegemier, G. A. and Innamorato, D. [1997] "Seismic retrofit of RC columns with continuous carbon fiber jackets," *Journal of Composites for Construction* **1**(2), 52–62.

Sezen, H., Elwood, K. J., Whittaker, A. S., Mosalam, K. M., Wallace, J. W. and Stanton, J. F. [2000] "Structural engineering reconnaissance of the August 17, 1999 earthquake: kocaeli (Izmit), Turkey Earthquake," PEER Report 2000/09, Pacific Earthquake Engineering Research Center, University of California, Berkeley, Berkeley, California.

Shi, Y., Hao, H. and Li, Z. X. [2008] "Numerical derivation of pressure–impulse diagrams for prediction of RC column damage to blast loads," *International Journal of Impact Engineering* **35** (11), 1213–1227.

Shi, Y., Li, Z. X. and Hao, H. [2009] "Bond slip modelling and its effect on numerical analysis of blast-induced responses of RC columns," *Structural Engineering and Mechanics* **32**(2), 251–267.

Shin, J., Scott, D. W., Stewart, L. K., Yang, C. S., Wright, T. R. and DesRoches, R. [2016] "Dynamic response of a full-scale reinforced concrete building frame retrofitted with FRP column jackets," *Engineering Structures* **125**, 244–253.

Spacone, E. and Limkatanyu, S. [2000] "Responses of reinforced concrete members including bond-slip effects," *ACI Structural Journal* **97**(6), 831–839.

Tabiei, A. and Wu, J. [2000] "Roadmap for crashworthiness finite element simulation of roadside safety structures," *Finite Elements in Analysis and Design* **34**(2), 145–157.

Woodson, S. C. and Baylot, J. T. [1999] "Structural collapse: quarter-scale model experiments," Technical Report SL-99-8, US Army Engineer Research and Development Center, Vicksburg, Mississippi.

Wright, T. R. [2015] "Full-scale seismic testing of a reinforced concrete moment frame using mobile shakers," Ph.D. thesis, School of Civil and Environmental Engineering, Georgia Institute of Technology, Atlanta, Georgia.

Wu, Y.F., & Wei, Y.Y. (2010). Effect of cross-sectional aspect ratio on the strength of CFRP-confined rectangular concrete columns. *Engineering Structures 32*(1): 32-45.

Wu, Y. and Crawford, J. E. [2015] "Numerical modeling of concrete using a partially associative plasticity model," *Journal of Engineering Mechanics* **141**(12), 04015051-1.

Xiao, Y., Wu, H. and Martin, G. R. [1999] "Prefabricated composite jacketing of RC columns for enhanced shear strength," *Journal Structureal Engineering* **125**(3), 255–264.

Yan, Z. and Pantelides, C. P. [2011] "Concrete column shape modification with FRP shells and expansive cement concrete," *Constr Build Mater* **25**(1), 396–405.

Youssf, O., ElGawady, M. A., Mills, J. E. and Ma, X. [2014] "Finite element modelling and dilation of FRP-confined concrete columns," *Engineering Structures 79*, 70–85.